



**HAL**  
open science

## Modeling Urban Impact on Zhengzhou Storm on July 20, 2021

Xiaowen Huang, Dashan Wang, Laurent Z X Li, Qi Li, Zhenzhong Zeng

► **To cite this version:**

Xiaowen Huang, Dashan Wang, Laurent Z X Li, Qi Li, Zhenzhong Zeng. Modeling Urban Impact on Zhengzhou Storm on July 20, 2021. *Journal of Geophysical Research: Atmospheres*, 2022, 127 (22), 10.1029/2022JD037387 . hal-04294491

**HAL Id: hal-04294491**

**<https://hal.science/hal-04294491>**

Submitted on 20 Nov 2023

**HAL** is a multi-disciplinary open access archive for the deposit and dissemination of scientific research documents, whether they are published or not. The documents may come from teaching and research institutions in France or abroad, or from public or private research centers.

L'archive ouverte pluridisciplinaire **HAL**, est destinée au dépôt et à la diffusion de documents scientifiques de niveau recherche, publiés ou non, émanant des établissements d'enseignement et de recherche français ou étrangers, des laboratoires publics ou privés.

## Modeling urban impact on Zhengzhou storm on July 20, 2021

Xiaowen Huang<sup>1</sup>, Dashan Wang<sup>1\*</sup>, Laurent Z. X. Li<sup>2</sup>, Qi Li<sup>3</sup>, Zhenzhong Zeng<sup>1\*</sup>

### Affiliations:

<sup>1</sup> School of Environmental Science and Engineering, Southern University of Science and Technology, Shenzhen, China

<sup>2</sup> Laboratoire de Météorologie Dynamique, Centre National de la Recherche Scientifique, Sorbonne Université, Ecole Normale Supérieure, Ecole Polytechnique, Paris, France

<sup>3</sup> School of Civil and Environmental Engineering, Cornell University, Ithaca, NY, USA

\*Correspondence to: zengzz@sustech.edu.cn (Z. Zeng); wangds6@sustech.edu.cn (D. Wang)

Manuscript for *Journal of Geophysical Research: Atmospheres*

### Key Points:

- A high-resolution model-based assessment of urban impacts on extreme rainfall for the severe “July-20 event” is presented
- The notable influences of urbanization in shifting the spatiotemporal rainfall patterns and causing storm stagnation are revealed
- Enhanced vertical updraft and moisture convergence dominate the differences in the center and south of Zhengzhou during the storm peak

**Abstract:** The heavy storm event that occurred from July 18 to July 22, 2021, in Henan province caused severe floods and casualties, especially in the provincial city, Zhengzhou. While the impacts of large-scale synoptic systems and local-scale orographic effects on the storm event have been studied, the role of urbanization remains unexplored. Using Weather Research and Forecasting model, the study designed two numerical experiments, differentiated by the presence of urban land cover, to investigate the urban impact on the storm event over Henan province, with a focus on Zhengzhou. Urbanization increases precipitation in the major urban area of Zhengzhou and its south, western Kaifeng, and western Xuchang, where the largest increases reach from 188.2 mm to 304.4 mm. Further investigation into Zhengzhou city reveals that urbanization leads to shifted precipitation center and stagnation in the major urban area, resulting in earlier peak rainfall time and more concentrated precipitation. Elevated surface temperature and sensible heat are identified before the peak rainfall arrives, which leads to increased planet boundary layer height, suggesting the contribution of the urban heat island effect. Thermal perturbation and increased surface roughness over urban areas promote vertical uplift and moisture convergence, increasing water vapor and forming storm system drags during the peak precipitation time, thus bringing earlier and higher amounts of precipitation to the major urban area and its south. The study calls for the consideration of the urban effect of extreme storm events and the precaution against waterlogging over urban areas in rapid-developing cities.

**Keywords:** land-atmosphere interaction, hydrometeorology, urbanization, extreme rainfall, coupled model simulation

## 1. Introduction

A record-breaking storm took place in Henan province of China from 00 UTC July 18 to 00 UTC July 22, 2021. The storm brought devastating floods and waterlogging to the province, with the precipitation center located in the provincial capital, Zhengzhou. The extreme event caused 292 deaths and 47 people missing to Zhengzhou city, associated with direct economic losses of 53.2 billion yuan (Yin et al., 2022). Zhengzhou meteorological station recorded accumulated rainfall of 817.3 mm during the storm episode, with maximum hourly rainfall of 201.9 mm at 08-09 UTC on July 20, which makes this exceptionally heavy precipitation episode widely known as the “July-20 event” in the scientific community and public media.

Previous studies have revealed the important role of large-scale synoptic systems in this extreme precipitation episode’s formation and development (Wei et al., 2022; Xu et al., 2022). The well-established Huanghuai cyclone (situated in southern Henan province first and slowly moved northward to western Henan province) enhanced a low-level jet with strong southwesterly flow, a crucial circulation for the initiation of the July-20 event. To the south, the two typhoons In-Fa and Cempaka (situated over the Philippine Sea and the South China Sea, respectively) created favorable conditions to transport abundant water vapor from the tropics to the storm area (Ran et al., 2021). In addition to synoptic conditions, local factors also contributed to precipitation intensification. For example, orographic lifting related to Mount Song in the southwest of Zhengzhou and Mount Taihang in the north was identified to make contributions to the heavy precipitation (Ran et al., 2021; Su et al., 2021). Beyond local orographic conditions, it is believed that other factors, such as land use and land cover properties, can also play a role in this extreme precipitation event (Pielke et al., 2011). Yet, limited attention has been paid to the potential impacts of local land properties on the record-breaking “July-20 event” (Luo et al., 2022).

Drastic land cover conversion has occurred in China in the past forty years and urban area expansion was one of the major types of land conversion (Liu et al., 2020). The most spectacular urban expansion was certainly in the low-lying coastal zone (e.g., agglomerations in the region of Beijing-Tianjin-Hebei, in the Yangtze River Delta and Pearl River Delta), but central China including Henan province has experienced accelerating urbanization since 2000 (Liu et al., 2014; Ning et al., 2018). Urban extent is highly relevant to precipitation modification through land-atmosphere interactions (Shepherd, 2005; Han et al., 2014). Previous studies, both analytical and numerical modeling, revealed a variety of inter-related mechanisms of urban environments that can alter the spatiotemporal features of extreme precipitation, including urban canopy effects, urban heat island effects, and urban aerosol effects (Thielen et al., 2000; Han & Baik, 2008; Rosenfeld et al., 2008). Consequently, urban settings can exert complex impacts on precipitation extremes. For example, they can enhance precipitation by favoring vertical motions, invigorating convective systems, and promoting moisture convergence (Rozoff et al., 2003). Oppositely, they can also reduce precipitation via convective available potential energy reduction and evapotranspiration decrease (Zhang et al., 2009; Georgescu et al., 2012). Furthermore, the magnitude of urban effects on extreme precipitation can be greatly influenced by diverse synoptic conditions and topographic settings, increasing the uncertainty of changing extreme precipitation characteristics at local scale (Freitag et al., 2018; Wang et al., 2021a). Urban-atmosphere interactions may display more

heterogeneous spatiotemporal variations of extreme precipitation than large-scale systems, and often contribute to extreme events. However, the underlying mechanisms that take responsibility for these events remain uncertain (Qian et al., 2022).

In recent years, the construction of Central Plains urban agglomeration has resulted in explosive urbanization in Henan province (Wang et al., 2020). Located in complex terrain, Henan province has experienced severe extreme precipitation events in the past. For example, a torrential storm lashed Henan province from July 18 to July 20, 2016, with maximum accumulated precipitation of 732 mm recorded, causing 1.67 million people on sufferance (Li et al., 2018). Despite several studies focusing on large metropolitan areas, such as Beijing, Shanghai, and the Pearl River Delta, few studies have investigated the urban impact on extreme precipitation in Henan, including the rapid-growing provincial capital, Zhengzhou, where the center of the urban agglomeration locates. Due to the diverse findings and conclusions in prior studies across different areas, the transferability of the research results from one place to another remains unsettled (Li et al., 2015; Yan et al., 2020; Wang J et al., 2021), confining the application of the conclusions in these metropolitan areas on Henan. As the population continues to densify in urban areas, cities are expected to face higher risks of extreme precipitation events (Kumar, 2021). Therefore, an investigation into the July-20 storm under recent urbanization is necessary and will provide important insights into urban hazard mitigation and future urbanization in this area.

In this study, the urbanization impacts on the severe “July-20 event” are investigated. Using numerical model simulation, we analyzed the urban effect on the spatiotemporal pattern of the storm by setting up different land cover types in contrast experiments. Furthermore, we focus on the urban area of Zhengzhou city, which has experienced extreme rainfall and significant societal losses, to investigate the potential mechanisms for the observed differences caused by urbanization.

## **2. Materials and Methods**

### **2.1 Coupled land-atmosphere model configuration**

The Advanced Research version 4.2.2 of the Weather Research and Forecasting (WRF-ARW) model developed by the National Center for Atmospheric Research was adopted to perform the numerical simulations. Being a non-hydrostatic, three-dimensional, and sophisticated mesoscale model, WRF has been widely used in various research, including regional climate research, hurricane research, and land-atmosphere interactions (Bukovsky & Karoly, 2009; Skamarock et al., 2019; Wang et al., 2021b). Noah Mosaic Land Surface Model (Li et al., 2013) was coupled with the WRF model to provide reasonable subgrid-scale variability and sensitivity in the land-atmosphere interactions (Wang et al., 2021b). Rooted in the Noah land surface scheme (Chen & Dudhia, 2001), the Noah mosaic considers various land covers in the calculation of fluxes and surface variables within each grid, which is different from the Noah scheme that only takes the dominant land cover into account. For experiments with urban land cover, the Single-Layer Urban Canopy Model was coupled for better simulation of thermodynamic characteristics and interactions between urban surface and atmosphere (Chen et al, 2011).

Three one-way nested domains were configured, with a grid spacing of 25 km, 5 km, and 1 km, respectively. The horizontal grids were 95×89 for the outer domain (D01), 150×150 for the middle (D02), and 220×220 for the innermost domain (D03). The outermost domain covered most of eastern China (Figure 1a). The innermost domain is located in the center of Henan province, covering most of the large cities of Henan province, for example, Zhengzhou, Luoyang, and Kaifeng (Figure 1b). The model contained 35 vertical levels, with the upper boundary to be 50 hPa. The initial and boundary conditions were provided by the fifth-generation reanalysis data (ERA5) of the European Centre for Medium-Range Weather Forecasts (ECMWF) with a spatial resolution of 0.25° and a temporal resolution of 1 h (Hersbach & Dee, 2016).

All simulations shared identical physical schemes (summarized in Table 1). The WRF Single-Moment 6-class scheme was chosen in microphysics as it is recommended for high-resolution simulations (Hong & Lim, 2006). The Rapid Radiative Transfer Model was applied in longwave radiation due to its efficient and accurate fluxes and heating calculation with the correlated- $k$  approach (Mlawer et al., 1997). Shortwave radiation used the Dudhia scheme which takes terrain slope and shadow effect on surface solar flux into consideration (Dudhia, 1989). The Yonsei University scheme was employed for planetary boundary layer, as it is able to parameterize turbulent vertical fluxes of momentum, heat, and constituents, both in the planetary boundary layer and the atmosphere (Hong et al., 2006). The Kain-Fritsch cumulus scheme was adopted for the simulation of convective cloud effects (Kain, 2004). Due to the fine grid spacing in D02 and D03, the cumulus scheme was turned off in the two domains (<10 km; Yang et al., 2021). The surface layer was simulated by the revised MM5 scheme (Jiménez et al., 2012).

## 2.2 Experimental design

Two numerical experiments were designed, namely CTRL and NoUrban, differentiated by the presence of urban land cover. As the default land cover in WRF, MODIS 30s land cover product was generated based on the year 2001 (Friedl et al., 2002), the dataset could not adequately represent the current land cover under such drastic urbanization in China (Li et al., 2014). Therefore, the “LANDUSEF” and “LU\_INDEX” parameters which were formerly calculated based on default MODIS land cover in the WRF model, were modified according to the WorldCover 2020 v100 product of 10 m resolution released by the European Space Agency (ESA) to more accurately generate the current land use over the study area. The product contains 11 classes of land cover in 2020 and shows an overall accuracy of 74.4%, with the highest accuracy measured in Asia (80.7%; Zanaga et al., 2021). The land cover in D03 included 8 of the 11 classes, namely, tree cover, shrubland, grassland, cropland, built-up, bare/sparse vegetation, permanent water bodies, and herbaceous wetland (Figure 1c). The urban built-up areas are mostly scattered, with the three densest areas located in eastern Luoyang, northeastern Zhengzhou, and western Kaifeng. The 10-m land cover data for 2020 was first aggregated into grids of the same grid spacing in WRF for each domain. The proportion of every class in each 25 km/5 km/1 km grid ( $f_{ESA}$ ) was calculated. Specifically, the 11 ESA classes were in correspondence with MODIS categories based on one-to-one, one-to-many, or many-to-one relationships (Table 2). For every class with a one-to-one relationship,

the modified fraction under MODIS categories ( $f_{M\_new}$ ) was calculated as:

$$f_{M\_new} = f_{ESA}. \quad (1)$$

In one-to-many relationships,  $f_{M\_new}$  was calculated based on the original MODIS fraction ( $f_{M\_ori}$ ) and  $f_{ESA}$ :

$$f_{M\_new,i} = f_{ESA} \times \frac{f_{M\_ori,i}}{\sum_{i=1}^n f_{M\_ori,i}}, \quad (2)$$

where  $n$  represented the number of MODIS classes and  $i$  ( $0 < i \leq n$ ) denoted the  $i$ th MODIS class in each one-to-many relationship. In many-to-one relationships,  $f_{M\_new}$  was formulated by:

$$f_{M\_new} = \sum_{j=1}^m f_{ESA,j}, \quad (3)$$

where  $m$  represented the number of ESA classes and  $j$  ( $0 < j \leq m$ ) denoted the  $j$ th ESA class in each many-to-one relationship. Finally, the ‘‘LANDUSEF’’ and ‘‘LU\_INDEX’’ parameters were updated with  $f_{M\_new}$  in the CTRL scenario. The NoUrban scenario is the same as CTRL but with modifications in the innermost domain, where the fraction of urban land cover was set to zero, and the fraction of other land cover types except water bodies increased proportionally. Compared with the CTRL scenario, grids in the NoUrban scenario that was previously dominated by urban land cover were mostly replaced by forests, croplands, and bare (Figure 2).

The simulation time was set up from 12 UTC on July 18 to 00 UTC on July 21, 2021, which covered the time of the heavy precipitation in Henan (Ran et al., 2021). The output interval was 1 h for the innermost domain. The first 12 hours were treated as spin-up, which would not be included in the analyses. Observed hourly precipitation data from 47 stations in D03 provided by the National Meteorological Information Center of the China Meteorological Administration (CMA) was applied to evaluate the model performance of the CTRL simulation. Correlation coefficient ( $r$ ) and root-mean-squared-error (RMSE) were used in the evaluation, and were calculated as follows:

$$r = \frac{\sum_{k=1}^N (Obs_k - \overline{Obs})(Sim_k - \overline{Sim})}{\sqrt{\sum_{k=1}^N (Obs_k - \overline{Obs})^2} \sqrt{\sum_{k=1}^N (Sim_k - \overline{Sim})^2}}, \quad (4)$$

$$RMSE = \sqrt{\frac{1}{N} \sum_{k=1}^N (Sim_k - Obs_k)^2}, \quad (5)$$

where  $Obs_k$  denoted the  $k$ th ( $0 < k \leq N$ ) observational data in overall  $N$  data and  $Sim_k$  denoted the  $k$ th simulated data.

### 3. Results

#### 3.1 Model validation

The CTRL simulation generally captures the spatial pattern in rainfall accumulation and the temporal evolution. The model result matches the observed rainfall pattern in eastern

Zhengzhou and other surrounding cities, such as Kaifeng and Xuchang, implying the reasonable performance of WRF in simulating the heavy rainfall episode (Figure 3a). It also successfully simulates the largest rainfall accumulation measured in Zhengzhou station (observed: 732 mm; simulated: 692 mm within 2 days). Although some model grids underestimate the rainfall amount (for example, grids of Xinmi station, Songshan station, and Gongyi station in western Zhengzhou), the simulation still shows a high spatial correlation with the observation ( $r = 0.61$ ; Figure 3b). In Zhengzhou city, the event's epicenter, the temporal evolution, as depicted over the eight meteorological stations, is well captured over the corresponding model grids, with even a higher agreement if compared to the accumulated rainfall (temporal correlation  $r = 0.79$ , RMSE = 5.1 mm). The model captures the rainfall variability during the whole study period, especially the first peak around 04 UTC on July 20, but generally underestimates the overall rainfall intensity and the second peak in 08-09 UTC (Figure 3c). The underestimation at the second peak is likely due to the decreasing simulated rainfall at Zhengzhou station, where the simulation is about half of the observation in 08-09 UTC (Figure 3d). However, the simulated rainfall peak time at Zhengzhou station greatly matches the observed peak time, and the rainfall variation is well captured with  $r = 0.72$  and RMSE = 20.6 mm.

### 3.2 Basic features of precipitation differences attributed to urbanization

The NoUrban simulation displays a similar rainfall spatial pattern as in CTRL, but with subtle differences (Figure 4a). The accumulated rainfall also shows a very high amount in Zhengzhou city, with the center shifted westward compared to CTRL. By carefully analyzing the difference between the two simulations, distinct precipitation increases are found near various urban areas, for example, in Zhengzhou's major urban area (MUA) and its south, also in western Kaifeng and western Xuchang (Figure 4b, CTRL-minus-NoUrban showing effects of urbanization). The accumulated precipitation increase can be up to 250.9 mm in the MUA and 304.4 mm in its south, accounting for 55.2% and 91.7% of total precipitation in the two-day study period in the NoUrban simulation, respectively. In Kaifeng and Xuchang, maximum increments reach 188.2 mm and 205.3 mm, respectively. The results show strong amplification of rainfall totals near urban areas and suggest important effects of urbanization.

To further confirm the effects of urbanization, we perform statistical analysis, based on the fraction of urban extent of all model grids in the whole area of Zhengzhou city, and in its MUA, respectively (boundaries shown in Figure 1c). Results, stratified into two groups of low and high urban fractions (0-0.2 versus 0.8-1), are shown in Figure 4c in the form of a probability density function. Model grids with higher urban extent are expected to have larger positive precipitation differences (Figure 4c). Those with low urban fraction (0-0.2) experience mean rainfall differences of -31.5 mm, with smaller variation (standard deviation [STD] = 85.6 mm). The density function shifts positively for grids of high urban fraction (0.8-1), with the mean value increasing to 29.7 mm and the standard deviation to 123.2 mm. The enhancing effect is more pronounced in the MUA of Zhengzhou, where low urban fraction areas have a mean rainfall difference of -72.7 mm and high urban density areas experience a mean difference of 109.6 mm (Figure 4c). Despite the rainfall amplification near urban areas, negative differences are also detected, especially for the west and the east side of the MUA, where the largest

difference surpasses -300 mm (dashed red line in Figure 4c). The negative differences are likely due to the shift of the precipitation center/maxima to the urban areas in the CTRL simulation compared with the NoUrban simulation (Figures 4a and 4b).

The temporal sequences of the CTRL and NoUrban simulations show distinct evolution, as shown in Figure 4d depicting the mean precipitation for the observation obtained over eight meteorological stations and corresponding model grids inside Zhengzhou city. Two peaks are found in the NoUrban simulation, one at 02 UTC on July 20 and another occurring between 09 UTC and 13 UTC on July 20 while in the CTRL scenario, precipitation becomes more concentrated and occurs earlier with one peak during 03-08 UTC on July 20, suggesting urban modification in the temporal evolution of precipitation. The temporal evolution is further investigated through Hovmöller diagrams with precipitation rate averaged over longitude in the domain (Figure 5). The diagrams allow the analysis of the precipitation life cycle as they capture the rainfall propagation in a zonal/longitudinal direction over time (Goines & Kennedy, 2018). The precipitation zone propagates from east to west before July 20 driven by the southeasterly and easterly flow. Influenced by the Huanghuai cyclone and orographic lifting, then the precipitation zone moves eastward and stagnates in the MUA of Zhengzhou for about 9 hours (from 06 UTC to 15 UTC on July 20), then continue moving eastward (Figure 5a). Meanwhile, another precipitation zone emerges at 114.5°E around 00 UTC on July 20 and moves westward, then merges with the precipitation in MUA, which may further enhance the precipitation. The stagnation in the CTRL simulation provides high-intensity rainfall over the urban area of Zhengzhou, with the maximum increasing intensity of 19.8 mm h<sup>-1</sup>, 4.8 times larger than the intensity in the NoUrban simulation (Figure 5c). The intensified precipitation is mitigated in the NoUrban simulation, where the rain is more evenly distributed and the peak time is delayed during the same period (Figure 5b).

### 3.3 Main drivers for the urbanization-induced precipitation differences

After the detailed description on the spatiotemporal structures of precipitation changes attributed to urbanization (stagnation of rainfall in the major urban area after a quickly-reached peak), we further investigate the precipitation characteristics between 06 UTC and 15 UTC on July 20, which covers the essential part of the heavy precipitation episode (Figure 6, two simulations separately). The precipitation in CTRL is firstly concentrated in Zhengzhou's MUA and its south (06-09 UTC). One center stagnates in Zhengzhou and another center spreads southward into Xuchang (09-12 UTC) and finally dissipates (12-15 UTC; Figures 6a, 6c, and 6e). In contrast to CTRL, heavy precipitation in NoUrban begins on the west edge of the MUA, then propagates eastward into Kaifeng, passing through the MUA without stagnation (Figures 6b, 6d, and 6f). The different moving speed explains the early peak of precipitation in CTRL. Notably, NoUrban experiences larger rainfall maxima in every 3-hour accumulation (for example, > 300 mm in Figure 6b) than CTRL does. However, due to the rapid propagation of the event, the overall precipitation accumulation is much higher in CTRL for Zhengzhou's MUA. The rapid propagation in NoUrban is also likely the reason to explain the large difference in rainfall rate between the two simulations for the time interval 03-09 UTC (Figure 4d) since the model grids corresponding to the weather stations in Zhengzhou partly miss the rapid-moving system in NoUrban.

Urban impact on precipitation is highly relevant to thermal perturbation, convective activities, and moisture. We observed a slightly increased 2-m temperature associated with enhanced sensible heat flux in the MUA of the Zhengzhou area before the storm peaks around the MUA (Figures 7a and 7b). The higher sensible heat flux likely elevates the planetary boundary layer height, favoring the city's subsequent convective motions at the peak time (Figure 7c). Notably, the two simulations present a rather small difference in maximum convective available potential energy (MCAPE), indicating limited urban impact on atmospheric stability under the strong synoptic background, which may not be the main driver for the urban-induced precipitation difference (Figure 7d).

The drag effects of increasing urban surface roughness seem to be the major contributor on the precipitation anomaly between the two simulations (Figure 7e). Larger friction velocity is observed in the MUA in the CTRL simulation than the NoUrban simulation before the storm peak, which triggers the subsequent effects on local circulation and moisture during the storm peak (Figure 7f). Between 06-09 UTC on July 20, enhanced upward motion is found in the MUA of Zhengzhou (Figure 8a). There are two enhanced updrafts, one in the western boundary of the MUA (ascending from 900 hPa), and the other appears in the center of MUA, associated with increasing water vapor. The ascending air motion brings a narrow band of moisture upward from the surface, forming enhanced water vapor covering the MUA above 850 hPa, which favors the heavy rainfall in the MUA due to strong convection. Meanwhile, decreased water vapor is identified from the ground to 600 hPa in the west of the MUA and later found below 800 hPa in the MUA area (09-12 UTC), associated with downward vertical wind (Figure 8b), indicating a more stable lower atmosphere in the city. The downdraft and reduced water vapor content help to explain the negative rainfall difference in the west and the western boundary of the MUA area. During 12-15 UTC, the urban surface continues to promote updraft from the near-surface at the eastern boundary of MUA to around 800 hPa in the MUA center (Figure 8c), which is in correspondence with the continuous rainfall in the MUA. Increasing water vapor concentrates on the top of the major urban area and its west, suggesting abundant moisture to the MUA. The increased water vapor over urban is also associated with enhanced moisture convergence (Figure 9). During the peak rainfall period (06-15 UTC 20 July), enhanced moisture convergence can be identified in the south boundary of the MUA and the south, which may explain the continuously concentrated water vapor and the associated precipitation over these areas.

#### 4. Discussion

The contrast between the two numerical simulations shows that urbanization led to shifted precipitation center, bringing earlier and more concentrated rainfall to the major urban area of Zhengzhou and its south in the “July-20” storm, which is consistent with previous studies of storms in Zhengzhou (Dong et al., 2019; Su et al., 2019). Further investigation reveals the possible roles of urban heat island (thermodynamic) and urban surface roughness (dynamic) in this storm. Observed elevated near-surface temperature and sensible heat before the storm peak increase the planetary boundary layer height, thus potentially promoting vertical motions and moisture convergence in the subsequent storm peak (Niyogi et al., 2011). However, thermal impacts on this storm event are likely of less importance compared with surface roughness

impact, as the similar study done by Debbage and Shepherd (2019). Aerodynamic drag due to increased surface roughness appears to be the dominant mechanism for urban influence in our analysis. Increasing friction velocity is responsible for the shifted precipitation center, as identified in our study and other studies (Ganeshan & Murtugudde, 2015; Zhang et al., 2018). Since the MUA is surrounded by scattered urban areas, these areas may provide additional aerodynamic drag to the storm propagation, thereby bringing more precipitation to the MUA and its south (Figure 1c). The aerodynamic drag further affects local circulation by enhancing updrafts and bringing abundant water vapor content to the MUA center, which explains the stagnation over the major urban area of Zhengzhou and the accompanying rainfall increase. Moreover, urban modification in moisture convergence over the regions is identified, which has also been confirmed in other studies (Argüeso et al., 2016; Li et al., 2021). The demonstration of urban surface roughness's impact on moisture transport indicates its effect on storm structure modification, which is in agreement with former studies (Shem & Shepherd, 2009; Zhang et al., 2018, Li et al., 2021).

It is noted that our research targets the urban impacts alone, but the extreme event can also be influenced through combining effects of urbanization and other factors, such as the topography. Prior studies have demonstrated the crucial role of topography in precipitation modification (Fairman et al., 2011; Houze, 2012; Navale & Singh, 2020). Cities located in complex terrain may be affected by complex interaction between urban-induced and terrain-induced circulations (Fernando, 2010). Frequent convergence could be produced at the urban interface in orographic-urban interactions (Shepherd, 2006). Freitag et al. (2018) suggested that terrain may amplify urban impacts on weather through persistent forcing of orographic flow. Precipitation amplification by urban-topography interactions may even surpass the effect of topography and urban alone (Yang et al., 2019). Research conducted on heavy precipitation that occurred in Zhengzhou on June 5, 2016, suggested that mountains in the northwest of Zhengzhou could generate gravity waves that promoted convection, leading to increased rainfall in the city (Su et al., 2019). Therefore, for Zhengzhou and its surrounding cities, it can be deduced that the mountains (Mount Song in the west of Zhengzhou, Mount Taihang in the north of Henan province, and the Funiu Mountain in the southwest of Henan province) may play an important role in urban-topography interactions and thus further modify the spatial and temporal patterns of the "July-20" storm event. Understanding urban-orographic interactions in "July-20" storm still requires additional studies, to be reported in future works.

The research highlights the critical role of the urban land cover effect in the severe storm event on July 20, which may provide insights into future storm analysis and call for precautions against urban waterlogging in Zhengzhou and other fast-growing cities in Henan province. Urban effect in the alteration of storm patterns can bring the precipitation center to the city and promote the stagnation of the storm, therefore increasing the risks of extreme precipitation and flash flood. The results can be further extended to cities worldwide that are rapidly expanding and facing similar synoptic conditions in extreme precipitation events. It is of note that the research may be affected by the lack of consideration of the urban aerosol effect as well as the uncertainties inside the atmospheric models. Additional research and improvement in models can provide further comprehensive and accurate assessments of extreme storm events.

## 5. Conclusions

The influence of urbanization on modifying the storm event that occurred on July 20, 2021, in Henan province was investigated, with a focus on the provincial city Zhengzhou. Two numerical simulations were designed and run from 12 UTC on July 18 to 00 UTC on July 21, one with the land cover of 2020 and the other replaced urban cover by other land types. Overall, the model accurately depicted the spatial and temporal patterns well. Urbanization increased accumulated precipitation in the major urban area of Zhengzhou and its south, western Xuchang, and western Kaifeng. In the provincial city Zhengzhou, urbanization led to shifted precipitation center to the major urban area and rainfall stagnation over and south of the urban area, resulting in earlier peak arrival time and longer storm system stagnation. Increased near-surface temperature and sensible heat in the major urban area were detected before peak precipitation began, suggesting the potential contribution of the urban heat island effect in the storm event. Looking into the peak rainfall time, the effect of urban surface roughness is believed to dominate the differences in the spatiotemporal pattern of the storm. The drag effects due to increased roughness provided pronounced vertical updrafts and increased water vapor content, associated with enhanced moisture convergence in areas with increasing rainfall. The study reveals the need for considering urban effects in storm events for developing cities and can be extended to future extreme storm events with similar synoptic conditions and urban settings, which may provide insights for urban hazard earlier-warning and mitigation.

## Acknowledgments

This study was supported by the National Natural Science Foundation of China (42071022, 42001321), the start-up fund provided by the Southern University of Science and Technology (29/Y01296122), and the Highlight Project on Water Security and Global Change of the Southern University of Science and Technology (G02296302). We thank the National Meteorological Information Centre of the China Meteorological Administration (CMA) for providing the precipitation data. We thank the Center for Computational Science and Engineering at the Southern University of Science and Technology for providing computing resources.

## Conflict of interest

The authors declare no competing interests.

## References

- Argüeso, D., Di Luca, A., & Evans, J. P. (2016). Precipitation over urban areas in the western Maritime Continent using a convection-permitting model. *Climate Dynamics*, 47(3), 1143-1159.
- Bukovsky, M. S., & Karoly, D. J. (2009). Precipitation simulations using WRF as a nested regional climate model. *Journal of Applied Meteorology and Climatology*, 48(10), 2152-2159.

- Chen, F., & Dudhia, J. (2001). Coupling an advanced land surface-hydrology model with the Penn State-NCAR MM5 modeling system. Part I: Model implementation and sensitivity. *Monthly Weather Review*, 129(4), 569-585.
- Chen, F., Kusaka, H., Bornstein, R., Ching, J., Grimmond, C. S. B., Grossman-Clarke, S., ... & Zhang, C. (2011). The integrated WRF/urban modelling system: development, evaluation, and applications to urban environmental problems. *International Journal of Climatology*, 31(2), 273-288.
- Debbage, N., & Shepherd, J. M. (2019). Urban influences on the spatiotemporal characteristics of runoff and precipitation during the 2009 Atlanta flood. *Journal of Hydrometeorology*, 20(1), 3-21.
- Dong, J., Liu, C., & Su, A. (2019) Impact of Urbanization on a Torrential Rain Process in Zhengzhou Region. *Journal of Arid Meteorology*, 37(6), 922-932.
- Dudhia, J. (1989). Numerical study of convection observed during the winter monsoon experiment using a mesoscale two-dimensional model. *Journal of the Atmospheric Sciences*, 46(20), 3077-3107.
- Fairman Jr, J. G., Nair, U. S., Christopher, S. A., & Mölg, T. (2011). Land use change impacts on regional climate over Kilimanjaro. *Journal of Geophysical Research: Atmospheres*, 116(D3).
- Fernando, H. J. S. (2010). Fluid dynamics of urban atmospheres in complex terrain. *Annual review of fluid mechanics*, 42, 365-389.
- Freitag, B. M., Nair, U. S., & Niyogi, D. (2018). Urban modification of convection and rainfall in complex terrain. *Geophysical Research Letters*, 45(5), 2507-2515.
- Friedl, M. A., McIver, D. K., Hodges, J. C., Zhang, X. Y., Muchoney, D., Strahler, A. H., ... & Schaaf, C. (2002). Global land cover mapping from MODIS: algorithms and early results. *Remote Sensing of Environment*, 83(1-2), 287-302.
- Ganeshan, M., & Murtugudde, R. (2015). Nocturnal propagating thunderstorms may favor urban “hot-spots”: A model-based study over Minneapolis. *Urban Climate*, 14, 606-621.
- Georgescu, M., Mahalov, A. and Moustauoui, M. (2012) Seasonal hydroclimatic impacts of Sun Corridor expansion. *Environmental Research Letters*, 7(3), 034026.
- Goines, D. C., & Kennedy, A. D. (2018). Precipitation From a Multiyear Database of Convection-Allowing WRF Simulations. *Journal of Geophysical Research: Atmospheres*, 123(5), 2424-2453.
- Han, J. Y., & Baik, J. J. (2008). A theoretical and numerical study of urban heat island-induced circulation and convection. *Journal of the Atmospheric Sciences*, 65(6), 1859-1877.
- Han, J. Y., Baik, J. J., & Lee, H. (2014). Urban impacts on precipitation. *Asia-Pacific Journal of Atmospheric Sciences*, 50(1), 17-30.
- Hersbach, H. & Dee, D. (2016). ERA5 reanalysis is in production. *ECMWF Newsletter*, 147, 7.
- Hong, S.-Y. & Lim, J., (2006). The WRF single-moment 6-class microphysics scheme (WSM6). *Asia-Pacific Journal of Atmospheric Sciences*, 42, 129-151.
- Hong, S.-Y., Noh, Y., & Dudhia, J. (2006). A new vertical diffusion package with an explicit treatment of entrainment processes. *Monthly Weather Review*, 134(9), 2318-2341.
- Houze Jr, R. A. (2012). Orographic effects on precipitating clouds. *Reviews of Geophysics*, 50(1).

- Jiménez, P. A., Dudhia, J., González-Rouco, J. F., Navarro, J., Montávez, J. P., & García-Bustamante, E. (2012). A revised scheme for the WRF surface layer formulation. *Monthly Weather Review*, 140(3), 898-918.
- Kain, J. S. (2004). The Kain-Fritsch convective parameterization: An update. *Journal of Applied Meteorology*, 43(1), 170-181.
- Kumar, P. (2021). Climate Change and Cities: Challenges Ahead. *Frontiers in Sustainable Cities*, 3, 5.
- Li, D., Bou-Zeid, E., Barlage, M., Chen, F., & Smith, J. A. (2013). Development and evaluation of a mosaic approach in the WRF-Noah framework. *Journal of Geophysical Research: Atmospheres*, 118, 11918-11935.
- Li, H., Wang, X., Zhang, X., Lü, L., & Xu, W. (2018). Analysis on Extremity and Characteristics of the 19 July 2016 Severe Torrential Rain in the North of Henan Province. *Meteorological Monthly*, 44(9), 1136-1147.
- Li, M., Song, Y., Huang, X., Li, J., Mao, Y., Zhu, T., ... & Liu, B. (2014). Improving mesoscale modeling using satellite-derived land surface parameters in the Pearl River Delta region, China. *Journal of Geophysical Research: Atmospheres*, 119(11), 6325-6346.
- Li, Q., Yang, J., & Yang, L. (2021). Impact of urban roughness representation on regional hydrometeorology: An idealized study. *Journal of Geophysical Research: Atmospheres*, 126(4), e2020JD033812.
- Li, Z., Yan, Z., Tu, K., & Wu, H. (2015). Changes of precipitation and extremes and the possible effect of urbanization in the Beijing metropolitan region during 1960-012 based on homogenized observations. *Advances in Atmospheric Sciences*, 32(9), 1173-1185.
- Liu, X., Huang, Y., Xu, X., Li, X., Li, X., Ciais, P., ... & Zeng, Z. (2020). High-spatiotemporal-resolution mapping of global urban change from 1985 to 2015. *Nature Sustainability*, 3(7), 564-570.
- Liu, J., Kuang, W., Zhang, Z., Xu, X., Qin, Y., Ning, J., ... & Chi, W. (2014). Spatiotemporal characteristics, patterns, and causes of land-use changes in China since the late 1980s. *Journal of Geographical Sciences*, 24(2), 195-210.
- Luo, Y., Zhang J., Yu M., Liang X., Xia R., Gao Y., ... & Yin J. (2022). On the influences of urbanization on the extreme rainfall over Zhengzhou on 20 July 2021: A convection-permitting ensemble modeling study. *Advances in Atmospheric Science*, in press. <http://www.iapjournals.ac.cn/aas/en/article/doi/10.1007/s00376-022-2048-8>.
- Mlawer, E. J., Taubman, S. J., Brown, P. D., Iacono, M. J., & Clough, S. A. (1997). Radiative transfer for inhomogeneous atmospheres: RRTM, a validated correlated-k model for the longwave. *Journal of Geophysical Research*, 102(D14), 16663-16682.
- Navale, A., & Singh, C. (2020). Topographic sensitivity of WRF-simulated rainfall patterns over the North West Himalayan region. *Atmospheric Research*, 242, 105003.
- Ning, J., Liu, J., Kuang, W., Xu, X., Zhang, S., Yan, C., ... & Ning, J. (2018). Spatiotemporal patterns and characteristics of land-use change in China during 2010-2015. *Journal of Geographical Sciences*, 28(5), 547-562.
- Niyogi, D., Pyle, P., Lei, M., Arya, S. P., Kishtawal, C. M., Shepherd, M., ... & Wolfe, B. (2011). Urban modification of thunderstorms: An observational storm climatology and model case study for the Indianapolis urban region. *Journal of Applied Meteorology and Climatology*, 50(5), 1129-1144.

- Pielke Sr, R. A., Pitman, A., Niyogi, D., Mahmood, R., McAlpine, C., Hossain, F., ... & de Noblet, N. (2011). Land use/land cover changes and climate: modeling analysis and observational evidence. *Wiley Interdisciplinary Reviews: Climate Change*, 2(6), 828-850.
- Qian, Y., Chakraborty, T. C., Li, J., Li, D., He, C., Sarangi, C., ... & Leung, L. R. (2022). Urbanization Impact on Regional Climate and Extreme Weather: Current Understanding, Uncertainties, and Future Research Directions. *Advances in Atmospheric Sciences*, 1-42.
- Ran, L. K., Li, S. W., Zhou, Y. S., Yang, S., Ma, S. P., Zhou, K., ..., Li, N. (2021). Observational analysis of the dynamic, thermal, and water vapor characteristics of the “7.20” extreme rainstorm event in Henan province, 2021. *Chinese Journal of Atmospheric Sciences*, 45(6), 1366-1383.
- Rosenfeld, D., Lohmann, U., Raga, G. B., O'Dowd, C. D., Kulmala, M., Fuzzi, S., ... & Andreae, M. O. (2008). Flood or drought: how do aerosols affect precipitation? *Science*, 321(5894), 1309-1313.
- Rozoff, C. M., Cotton, W. R., & Adegoke, J. O. (2003). Simulation of St. Louis, Missouri, land use impacts on thunderstorms. *Journal of Applied Meteorology*, 42(6), 716-738.
- Shem, W., & Shepherd, M. (2009). On the impact of urbanization on summertime thunderstorms in Atlanta: Two numerical model case studies. *Atmospheric Research*, 92(2), 172-189.
- Shepherd, J. M. (2005). A review of current investigations of urban-induced rainfall and recommendations for the future. *Earth Interactions*, 9(12), 1-27.
- Shepherd, J. M. (2006). Evidence of urban-induced precipitation variability in arid climate regimes. *Journal of Arid Environments*, 67(4), 607-628.
- Skamarock, W. C., Klemp, J. B., Dudhia, J., Gill, D. O., Liu, Z., Berner, J. et al. (2019). A description of the advanced research WRF Version 4 *NCAR Tech. Note NCAR/TN-556+STR*. 145 pp.
- Su, A., Lü, X., Cui, L., Li, Z., Xi, L., & Su, H. (2021). Prediction and test of optimal integrated precipitation based on similar spatial distribution of precipitation. *Torrential Rain and Disasters*, 40(5), 445-454.
- Su, A., Shi, D., & Ge, X. (2019). Numerical simulation of the influence from urbanization and orography on a severe rainfall event in Zhengzhou. *Transactions of Atmospheric Sciences*, 42(3), 434-446.
- Thielen, J., Wobrock, W., Gadian, A., Mestayer, P. G., & Creutin, J. D. (2000). The possible influence of urban surfaces on rainfall development: a sensitivity study in 2D in the meso- $\gamma$ -scale. *Atmospheric Research*, 54(1), 15-39.
- Wang, D., Wang, X., Liu, L., Wang, D., & Zeng, Z. (2021a). Urban signatures in the spatial clustering of precipitation extremes over mainland China. *Journal of Hydrometeorology*, 22(3), 639-656.
- Wang, D., Wu, J., Huang, M., Li, L. Z., Wang, D., Lin, T., ... & Zeng, Z. (2021b). The Critical Effect of Subgrid-Scale Scheme on Simulating the Climate Impacts of Deforestation. *Journal of Geophysical Research: Atmospheres*, 126(17), e2021JD035133.
- Wang, J., Chen, F., Doan, Q. V., & Xu, Y. (2021). Exploring the effect of urbanization on hourly extreme rainfall over Yangtze River Delta of China. *Urban Climate*, 36, 100781.
- Wang, J., Hu, C., Ma, B., & Mu, X. (2020). Rapid urbanization impact on the hydrological processes in Zhengzhou, China. *Water*, 12(7), 1870.

- Wei, P., Xu, X., Xue, M., Zhang, C., Wang, Y., Zhao, K., ... & Zhu, K. (2022). On the key dynamical processes supporting the 21.7 Zhengzhou record-breaking hourly rainfall in China. *Advances in Atmospheric Sciences*.
- Xu, H., Duan, Y., & Xu, X. (2022). Indirect effects of binary typhoons on an extreme rainfall event in Henan province, China from 19 to 21 July 2021. Part I: Ensemble-based analysis. *Journal of Geophysical Research: Atmospheres*, e2021JD036265.
- Yan, M., Chan, J. C., & Zhao, K. (2020). Impacts of urbanization on the precipitation characteristics in Guangdong Province, China. *Advances in Atmospheric Sciences*, 37(7), 696-706.
- Yang, L., Ni, G., Tian, F., & Niyogi, D. (2021). Urbanization exacerbated rainfall over European suburbs under a warming climate. *Geophysical Research Letters*, 48, e2021GL095987.
- Yang, L., Smith, J., & Niyogi, D. (2019). Urban impacts on extreme monsoon rainfall and flooding in complex terrain. *Geophysical Research Letters*, 46(11), 5918-5927.
- Yin, J., Gu, H., Liang, X., Yu, M., Sun, J., Xie, Y., ... & Wu, C. (2022). A possible dynamic mechanism for rapid production of the extreme hourly rainfall in Zhengzhou city on 20 July 2021. *Journal of Meteorological Research*, 36(1), 6-25.
- Zhang, C. L., Chen, F., Miao, S. G., Li, Q. C., Xia, X. A., & Xuan, C. Y. (2009). Impacts of urban expansion and future green planting on summer precipitation in the Beijing metropolitan area. *Journal of Geophysical Research: Atmospheres*, 114(D2).
- Zhang, W., Villarini, G., Vecchi, G. A., & Smith, J. A. (2018). Urbanization exacerbated the rainfall and flooding caused by hurricane Harvey in Houston. *Nature*, 563(7731), 384-388.
- Zanaga, D., Van De Kerchove, R., De Keersmaecker, W., Souverijns, N., Brockmann, C., Quast, R., ... & Arino, O. (2021). ESA WorldCover 10 m 2020 v100.

**Table Legends.**

**Table 1. Overview of WRF physical schemes.**

**Table 2. Relationships between ESA classification and MODIS 21-category land use categories.** The bold number denotes the original map code.

1 **Table 1. Overview of WRF physical schemes.**

Physics option	Parameterization scheme
Microphysics	WSM 6-class scheme
Longwave radiation	RRTM scheme
Shortwave radiation	Dudhia scheme
Planet boundary layer	Yonsei University scheme
Cumulus	Kain-Fritsch scheme
Land surface	Noah mosaic land surface model
Urban surface	Single-layer UCM
Surface layer	Revised MM5 scheme

2

3 **Table 2. Relationships between ESA classification and MODIS 21-category land use**  
 4 **categories.** The bold number denotes the original map code in the classes.

Relationship	ESA category and code	MODIS category and code
One-to-one	<b>50</b> Built-up	<b>13</b> Urban and Built-up
	<b>70</b> Snow and Ice	<b>15</b> Snow and Ice
	<b>60</b> Bare/sparse Vegetation	<b>16</b> Barren or Sparsely Vegetated
One-to-many	<b>10</b> Tree Cover	<b>1</b> Evergreen Needleleaf Forest
		<b>2</b> Evergreen Broadleaf Forest
		<b>3</b> Deciduous Needleleaf Forest
		<b>4</b> Deciduous Broadleaf Forest
	<b>20</b> Shrubland	<b>5</b> Mixed Forest
		<b>6</b> Closed Shrublands
		<b>7</b> Open Shrublands
		<b>8</b> Woody Savannas
		<b>9</b> Savannas
	<b>30</b> Grassland	<b>10</b> Grasslands
		<b>12</b> Croplands
		<b>14</b> Cropland/natural vegetation mosaic
		<b>17</b> Water
<b>40</b> Cropland	<b>21</b> Lake	
	<b>18</b> Wooded Tundra	
<b>80</b> Permanent Water Bodies	<b>19</b> Mixed Tundra	
	<b>20</b> Barren Tundra	
	<b>90</b> Herbaceous Wetland	
	<b>11</b> Permanent Wetlands	
Many-to-one	<b>95</b> Mangroves	

5

6 **Figure Legends.**

7 **Figure 1. Study regions.** (a) Boundaries of the three one-way nested domains D01, D02, and  
8 D03; (b) Topography and major cities in domain 3; (c) The spatial pattern of land cover/land  
9 use types and the location of meteorological stations (black dots) in domain 3. The large  
10 rectangle (dashed line) outlines Zhengzhou city and the small rectangle (solid line) outlines the  
11 major urban area (MUA).

12 **Figure 2. Dominant land category for (a) CTRL and (b) NoUrban simulations in D03.**

13 **Figure 3. Model validation.** (a) Rainfall accumulation of CTRL simulation between 00 UTC  
14 19 July to 00 UTC 21 July, bold line outlines the boundary of Zhengzhou prefectural-level city,  
15 ‘ZZ’, ‘XM’, ‘SS’, and ‘GY’ denote Zhengzhou station, Xinmi station, Songshan station, and  
16 Gongyi station, respectively; (b) Scatter plots of rainfall amount between stations in domain 3  
17 and the corresponding model grids accumulated from 00 UTC 19 July to 00 UTC 21 July; (c)  
18 Time series of hourly rain rate ( $\text{mm h}^{-1}$ ) averaged over the 8 stations inside Zhengzhou city  
19 (black line) and corresponding model grids (blue line) from the CTRL simulation; (d) Time  
20 series of hourly rain rate ( $\text{mm h}^{-1}$ ) of Zhengzhou (‘ZZ’) station (brown line) and corresponding  
21 model grid (red line) from the CTRL simulation.

22 **Figure 4. Spatial and temporal patterns.** (a) Rainfall accumulation of NoUrban simulation  
23 between 00 UTC 19 July to 00 UTC 21 July; (b) Differences in rainfall accumulation between  
24 the two simulations (CTRL minus NoUrban). (c) Density curve for rainfall differences of  
25 model grids in Zhengzhou city (blue line; dash rectangle outlined in Figure 1c) and major urban  
26 area of Zhengzhou (MUA; red line; solid rectangle outlined in Figure 1c) under different urban  
27 percentage in model grids (0-0.2: dash line; 0.8-1: solid line). (d) Time series of hourly rainfall  
28 rate ( $\text{mm h}^{-1}$ ) averaged over the 8 stations inside Zhengzhou city (grey line), and the  
29 corresponding model grids from the CTRL simulation (blue line) and NoUrban simulation (red  
30 line).

31 **Figure 5. Hovmöller diagrams of hourly rainfall rate (shading,  $\text{mm h}^{-1}$ ) for (a) CTRL, (b)  
32 NoUrban simulations, and (c) their differences from 00 UTC 19 July to 00 UTC 21 July.**  
33 The rainfall rate is averaged in longitude within domain 3 for each hour. The vertical axis  
34 represents time and the horizontal axis represents longitude. Dotted lines denote 06 UTC and  
35 15 UTC on July 20. Dashed lines represent the major urban area of Zhengzhou (shown in  
36 Figure 1c). The precipitation zone is circled and the vector denotes its direction of propagation.

37 **Figure 6. Rainfall accumulation for CTRL and NoUrban simulation in (a-b) 06 UTC-09  
38 UTC 20 July, (c-d) 09 UTC-12 UTC 20 July, and (e-f) 12 UTC-15 UTC 20 July.** Vectors  
39 denote wind field at 700 hPa. Dashed lines represent the major urban area of Zhengzhou (shown  
40 in Figure 1c).

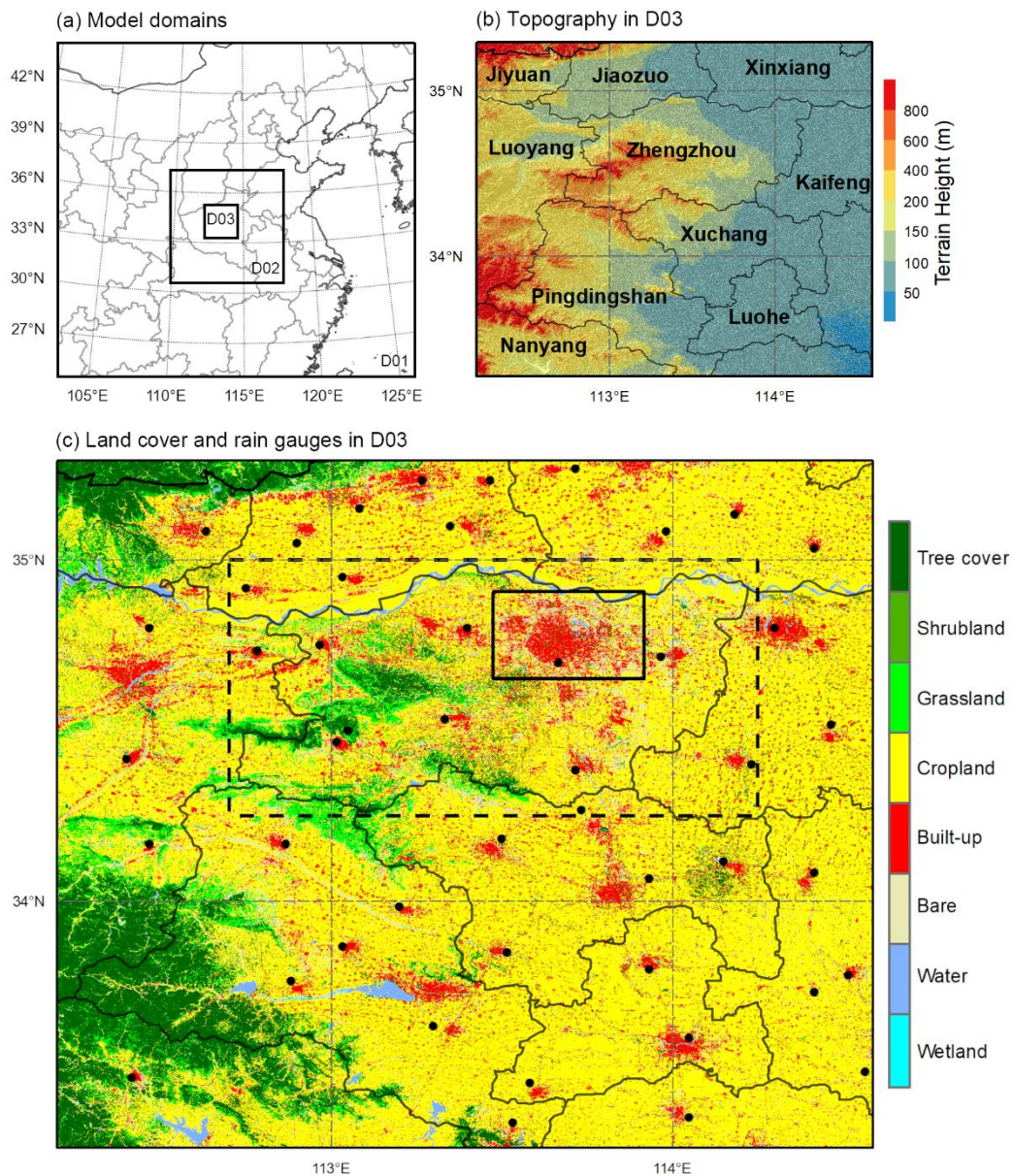
41 **Figure 7. CTRL-NoUrban differences of (a) 2-m temperature, (b) sensible heat flux, (c)  
42 planetary boundary layer height, (d) maximum convective available potential energy, (e)  
43 roughness length, and (f) friction velocity between 02 and 06 UTC of 20 July in Zhengzhou.**  
44 Dashed lines represent the major urban area of Zhengzhou (shown in Figure 1c).

45 **Figure 8. Averaged vertical profiles.** 3-hour-averaging vertical profiles of CTRL-NoUrban  
46 differences between (a) 06-09 UTC, (b) 09-12 UTC, and (c) 12-15 UTC on 20 July averaged

47 in longitude inside the Zhengzhou area. Shading represents differences in water vapor mixing  
48 ratio ( $\text{g kg}^{-1}$ ) and vectors denote composite horizontal and vertical wind (vertical wind shown  
49 has been multiplied by 10). Dashed lines represent the major urban area of Zhengzhou (shown  
50 in Figure 1c).

51 **Figure 9. CTRL-NoUrban differences of moisture convergence at 900 hPa (unit:  $\text{g kg}^{-1} \text{s}^{-1}$ ) for (a) 06-09 UTC, (b) 09-12 UTC, and (c) 12-15 UTC of 20 July.** Positive (negative)  
52 values indicate convergence (divergence). Dashed lines represent the major urban area of  
53 Zhengzhou (shown in Figure 1c).

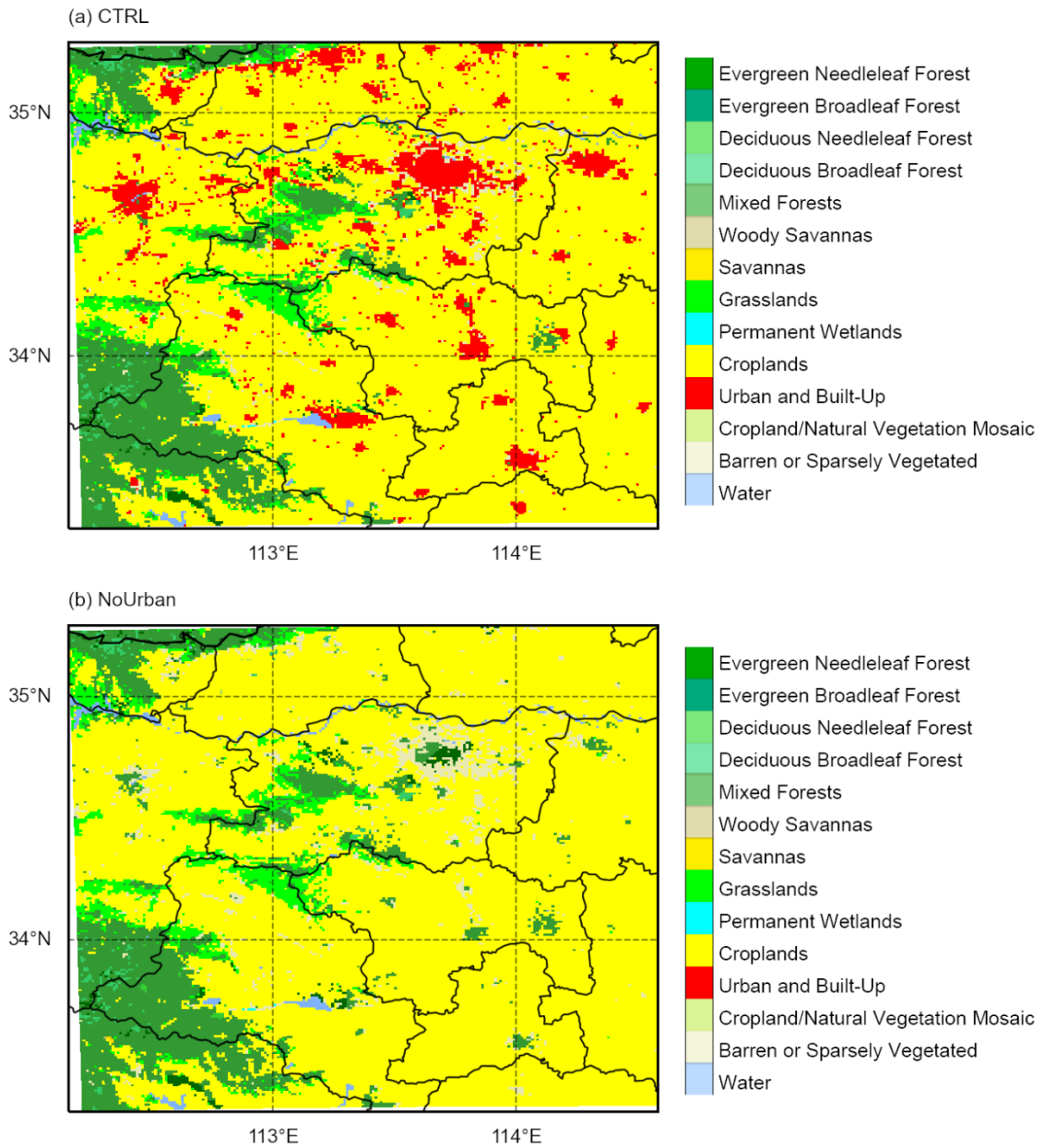
55



56

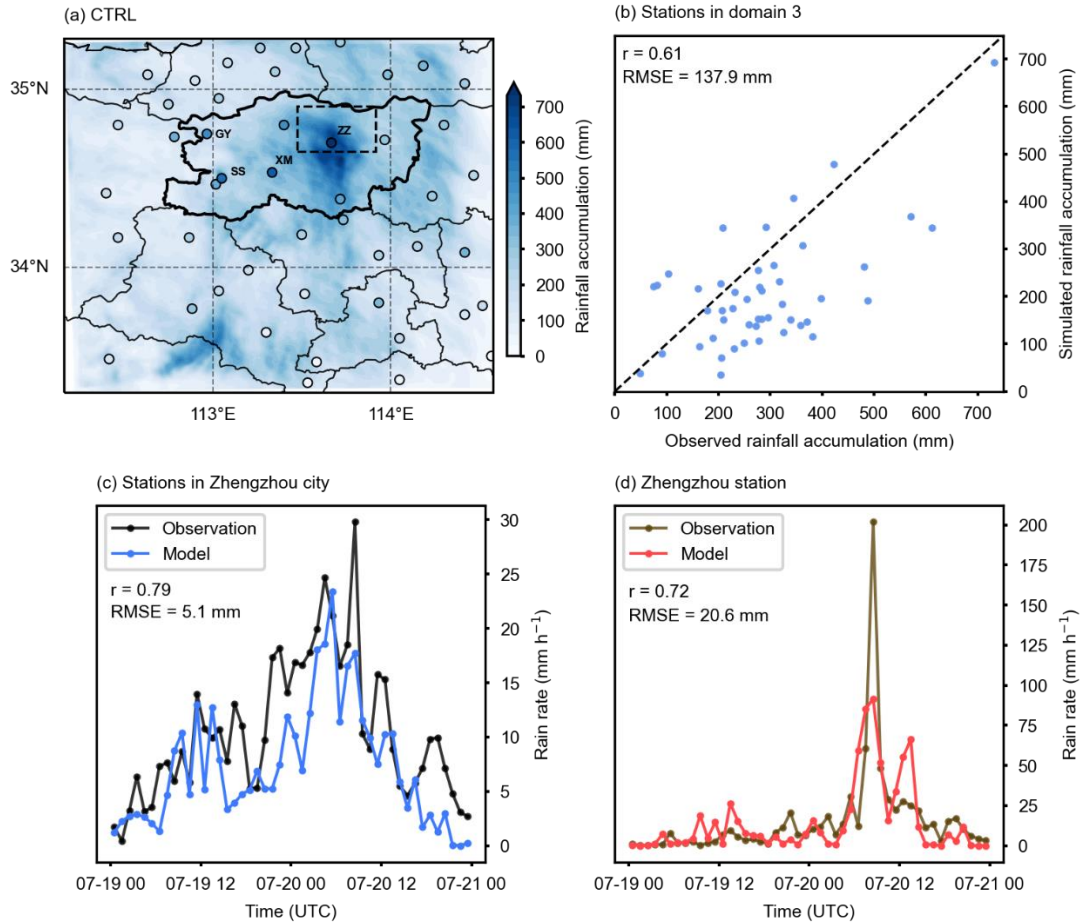
57 **Figure 1. Study region, surface properties and model domains.** (a) Boundaries of the three  
 58 one-way nested domains D01, D02, and D03; (b) Topography and major cities in domain 3; (c)  
 59 The spatial pattern of land cover/land use types and the location of meteorological stations  
 60 (black dots) in domain 3. The large rectangle (dashed line) outlines Zhengzhou city and the  
 61 small rectangle (solid line) outlines the major urban area (MUA).

62



63

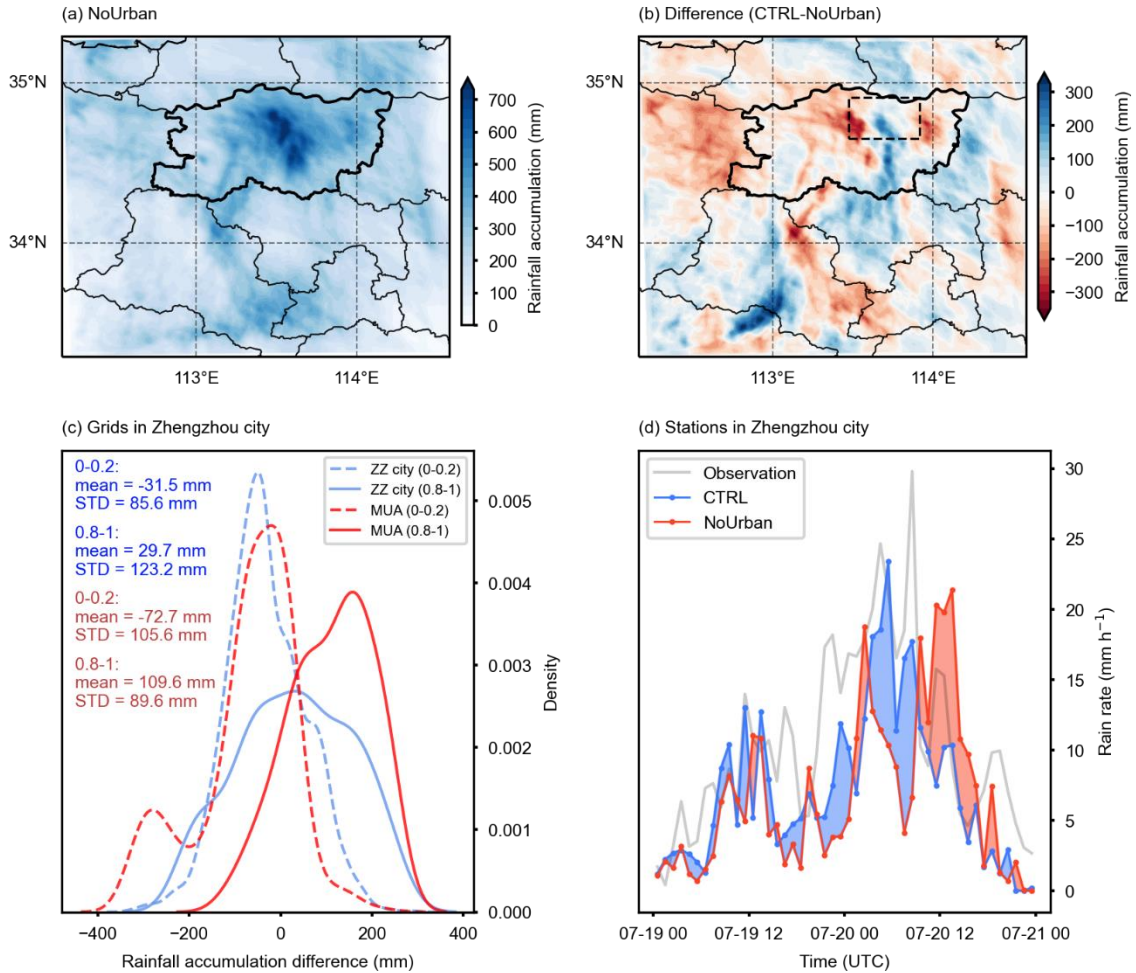
64 **Figure 2. Dominant land category for (a) CTRL and (b) NoUrban simulations in D03.**



65

66 **Figure 3. Model validation.** (a) Rainfall accumulation of CTRL simulation between 00 UTC  
 67 19 July to 00 UTC 21 July, bold line outlines the boundary of Zhengzhou prefectural-level city,  
 68 'ZZ', 'XM', 'SS', and 'GY' denote Zhengzhou station, Xinmi station, Songsshan station, and  
 69 Gongyi station, respectively; (b) Scatter plots of rainfall amount between stations in domain 3  
 70 and the corresponding model grids accumulated from 00 UTC 19 July to 00 UTC 21 July; (c)  
 71 Time series of hourly rainfall rate ( $\text{mm h}^{-1}$ ) averaged over the 8 stations inside Zhengzhou city  
 72 (black line) and corresponding model grids (blue line) from the CTRL simulation; (d) Time  
 73 series of hourly rainfall rate ( $\text{mm h}^{-1}$ ) of Zhengzhou ('ZZ') station (brown line) and  
 74 corresponding model grid (red line) from the CTRL simulation.

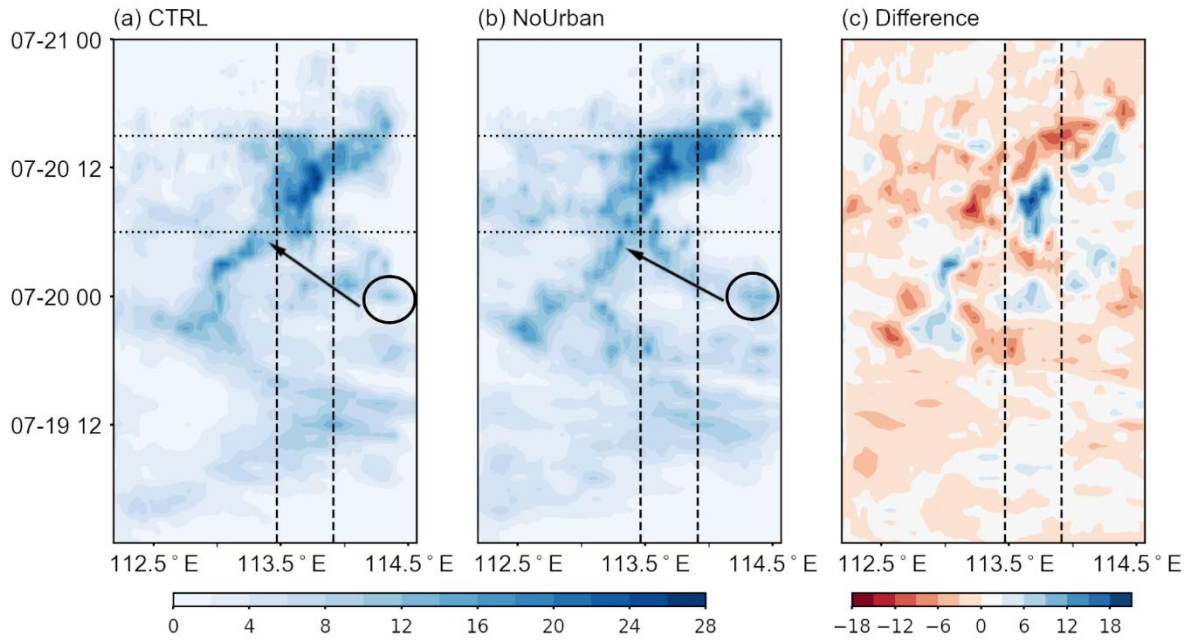
75



76

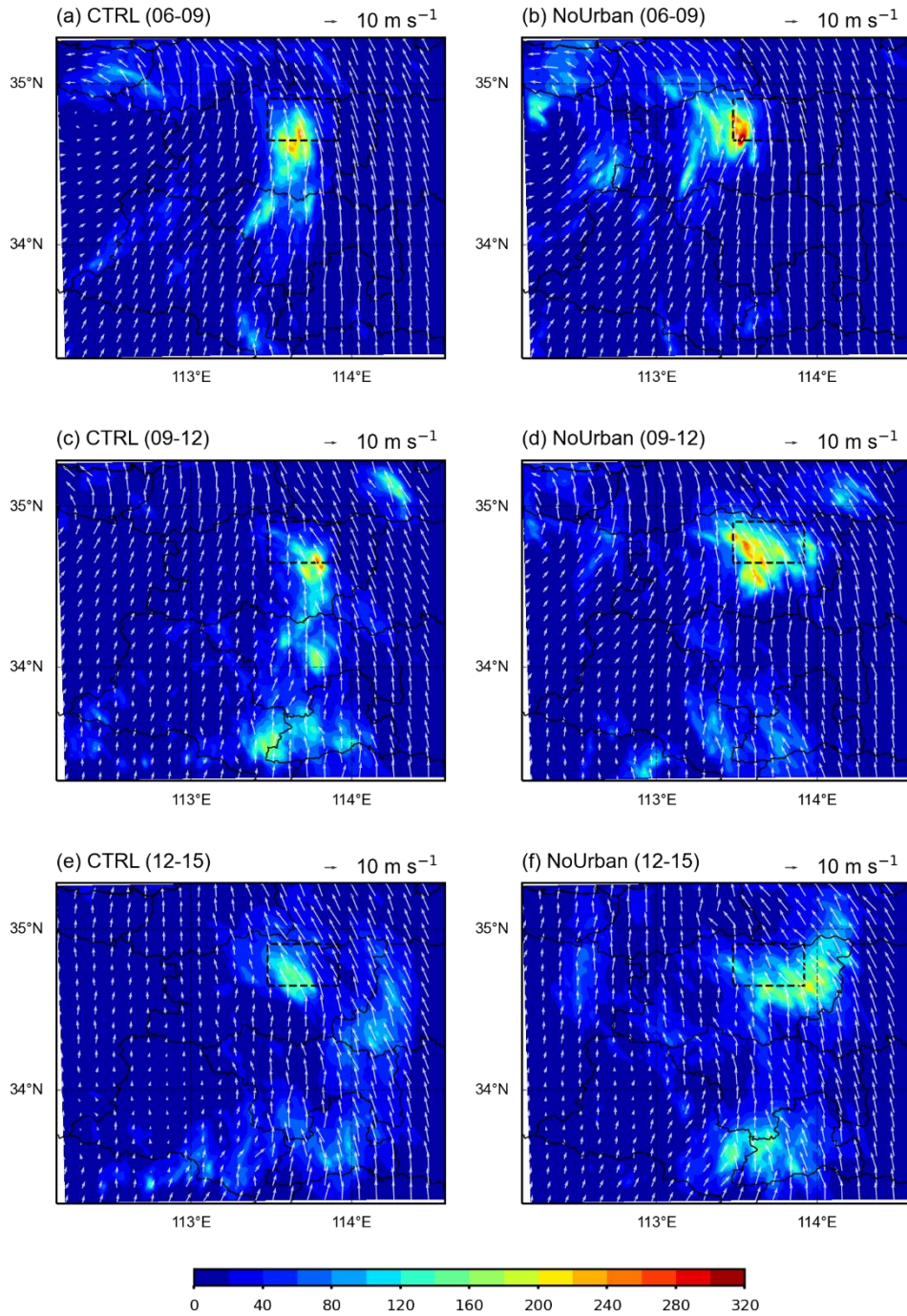
77 **Figure 4. Spatial and temporal patterns.** (a) Rainfall accumulation of NoUrban simulation  
 78 between 00 UTC 19 July to 00 UTC 21 July; (b) Differences in rainfall accumulation between  
 79 the two simulations (CTRL minus NoUrban). (c) Density curve for rainfall differences of  
 80 model grids in Zhengzhou city (blue line; dash rectangle outlined in Figure 1c) and major urban  
 81 area of Zhengzhou (MUA; red line; solid rectangle outlined in Figure 1c) under different urban  
 82 percentage in model grids (0-0.2: low urban density in dashed line; 0.8-1: high urban density  
 83 in solid line). (d) Time series of hourly rainfall rate (mm h<sup>-1</sup>) averaged over the 8 stations inside  
 84 Zhengzhou city (grey line), and the corresponding model grids from the CTRL simulation (blue  
 85 line) and NoUrban simulation (red line).

86



87

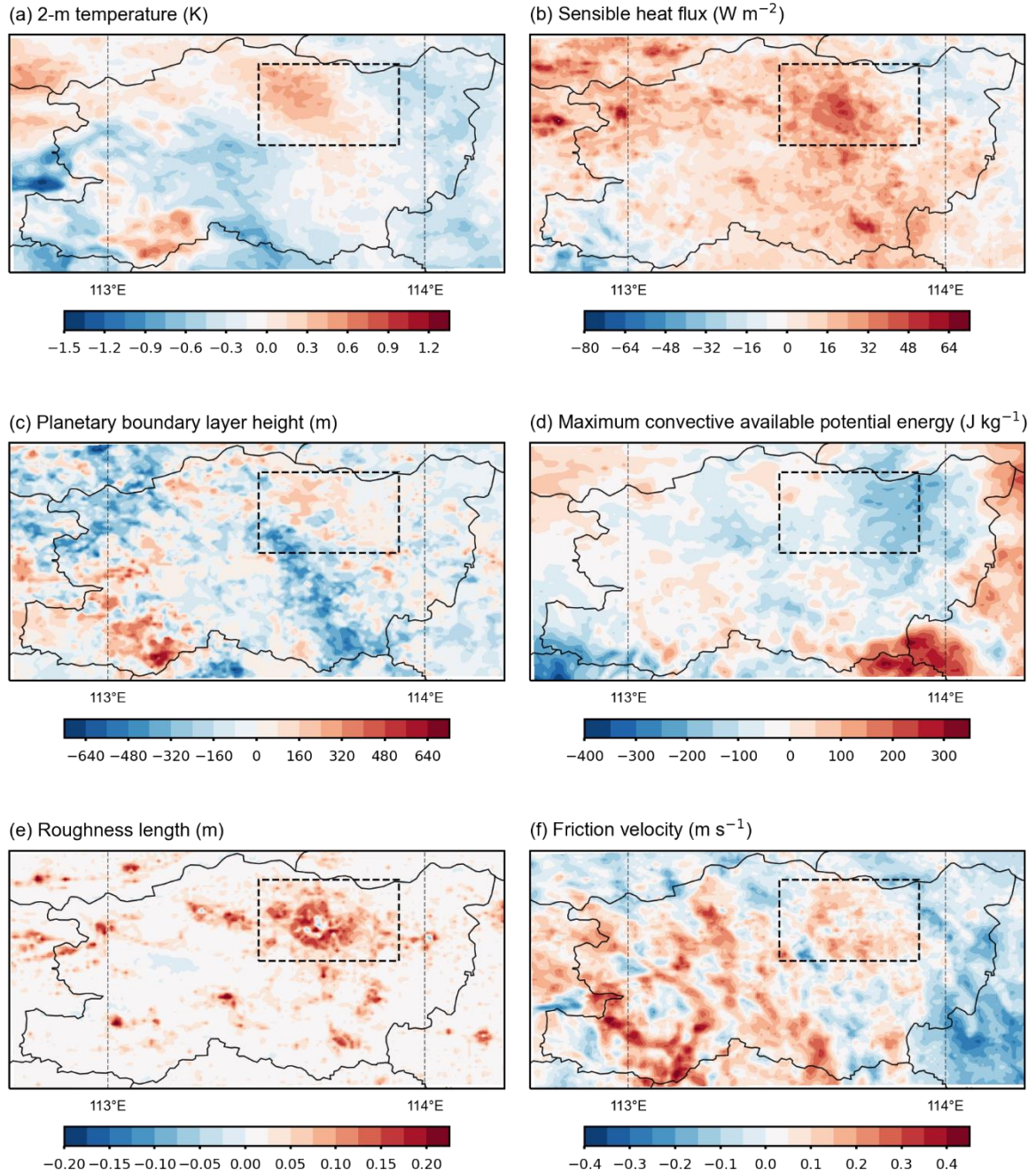
88 **Figure 5. Hovmöller diagrams of hourly rainfall rate (shading,  $\text{mm h}^{-1}$ ) for (a) CTRL, (b)**  
 89 **NoUrban simulations, and (c) their differences from 00 UTC 19 July to 00 UTC 21 July.**  
 90 The rainfall rate is averaged in longitude within domain 3 for each hour. The vertical axis  
 91 represents time and the horizontal axis represents longitude. Dotted lines denote 06 UTC and  
 92 15 UTC on July 20. Dashed lines represent the major urban area of Zhengzhou (shown in  
 93 Figure 1c). The precipitation zone is circled and the vector denotes its direction of propagation.



94

95 **Figure 6. Rainfall accumulation for CTRL and NoUrban simulations in (a-b) 06 UTC-09**  
 96 **UTC 20 July, (c-d) 09 UTC-12 UTC 20 July, and (e-f) 12 UTC-15 UTC 20 July.** Vectors  
 97 denote wind field at 700 hPa. Dashed lines represent the major urban area of Zhengzhou (shown  
 98 in Figure 1c).

99



100

101

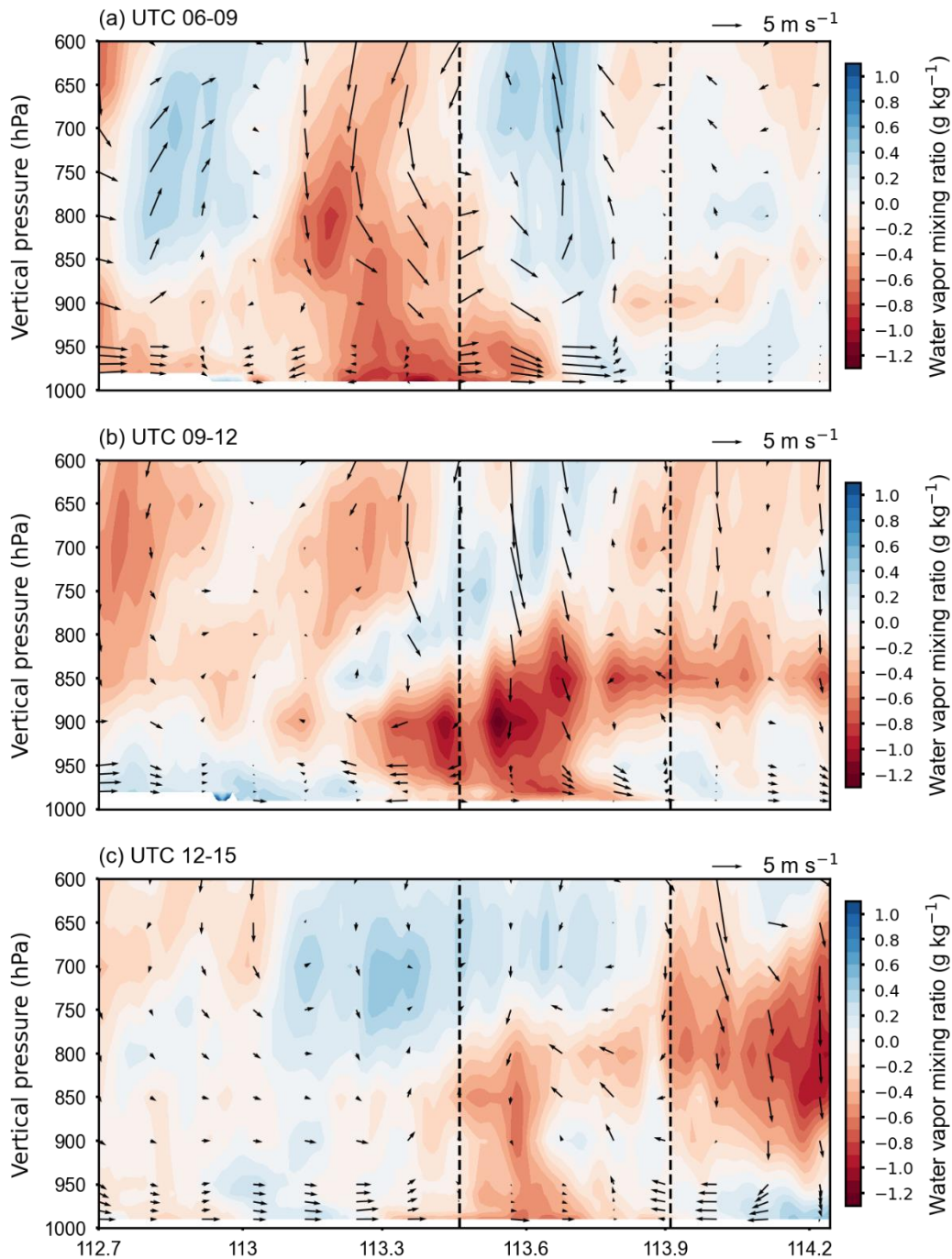
102

103

104

105

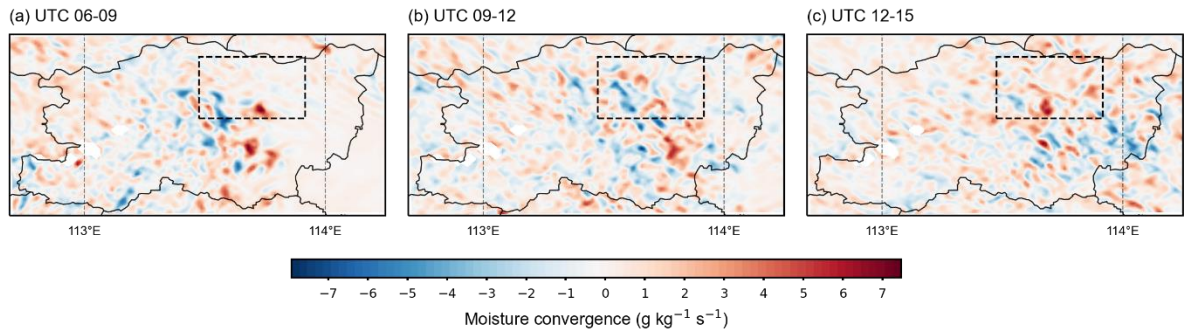
**Figure 7. CTRL-NoUrban differences of (a) 2-m temperature, (b) sensible heat flux, (c) planetary boundary layer height, (d) maximum convective available potential energy, (e) roughness length, and (f) friction velocity between 02 and 06 UTC of 20 July in Zhengzhou. Dashed lines represent the major urban area of Zhengzhou (shown in Figure 1c).**



106

107 **Figure 8. Averaged vertical profiles.** 3-hour-averaging vertical profiles of CTRL-NoUrban  
 108 differences between (a) 06-09 UTC, (b) 09-12 UTC, and (c) 12-15 UTC on 20 July averaged  
 109 in longitude inside the Zhengzhou area. Shading represents differences in water vapor mixing  
 110 ratio ( $\text{g kg}^{-1}$ ) and vectors denote composite horizontal and vertical winds (vertical wind  
 111 multiplied by 10). Dashed lines represent the major urban area of Zhengzhou (shown in Figure  
 112 1c).

113



114

115 **Figure 9. CTRL-NoUrban differences of moisture convergence at 900 hPa (unit:  $\text{g kg}^{-1} \text{s}^{-1}$ ) for (a) 06-09 UTC, (b) 09-12 UTC, and (c) 12-15 UTC of 20 July. Positive (negative)**  
 116 **values indicate convergence (divergence). Dashed lines represent the major urban area of**  
 117 **Zhengzhou (shown in Figure 1c).**

119